Polarization Efficiency Optimization of Freeform Liquid-Crystal Polarization Imaging Optics

Chunyang Pei*, Jiacheng Weng*, Guangyin Hu*, Rengmao Wu*, Haifeng Li* and Xu Liu*

*** State Key Laboratory of Extreme Photonics and Instrumentation, Zhejiang University, Hangzhou, China**

Abstract

Freeform Liquid-Crystal Imaging Optics (LPIOs) have attracted significant interest in near-eye displays, yet their polarization-sensitive nature causes diffraction efficiency variations under changing polarization states, leading to nonuniform performance. This study introduces an approach for polarization efficiency optimization of freeform LPIOs. An optimal balance between aberration correction and efficiency control can be achieved by optimizing the flexible phase profiles of freeform LPIOs. Validated through an augmented reality display system example, this work demonstrates the potential to advance freeform LPIO applications in optics and photonics.

Author Keywords

Freeform liquid-crystal polarization imaging optics; efficiency optimization; liquid-crystal polarization optical elements; 4×4 matrix method

1. Introduction

Liquid-crystal polarization imaging optics (LPIOs), with their strong polarization sensitivity, transparency, portability and broad spectral and angular response bandwidths, have attracted significant interest in next-generation interactive displays like augmented reality (AR) and virtual reality (VR) [1-3]. To enhance aberration correction and efficiency optimization of LPIOs, freeform liquid-crystal polarization imaging optics (LPIOs), the LPIOs with a freeform phase profile, is proposed in our previous work by incorporating freeform wavefronts during the exposure process of LPIOs [4]. By combining the advantages of freeform optics and LPIOs, freeform LPIOs can be used to build systems with high imaging performance, a compact form factor, and a flexible optical geometry.

However, the efficiency simulation of freeform LPIOs in prior studies relied on coupled wave theory [5], which calculates efficiency based on phase mismatch between the k vectors of the reference light, object light, and grating vector. While computationally efficient, this method fails to account for the polarization state of emitted light, a critical factor for accurately simulating and optimizing efficiency of multiple optics systems incorporating freeform LPIOs. On the other hand, methods like finite element method (FEM) [6] and finite-difference time-domain (FDTD) [7] are computationally intensive due to the structural complexity of freeform LPIOs and the iterative optimization required for aberration correction and efficiency optimization. Meanwhile, as AR display is advancing toward large diffraction angles and broad field of view, the finite bandwidth of freeform LPIOs further emphasizes the need for polarization efficiency optimization.

In this study, we developed an approach for polarization efficiency optimization of freeform LPIOs. Fast and accurate simulation of both polarization state and diffraction efficiency for each single beam can be realized based on the self-built 4×4 matrix module. To validate its effectiveness, we designed an AR display system comprising two freeform LPIOs and a reflective mirror. Using our method, the system efficiency improved significantly, from 59.81% to 88.21%, while field uniformity enhanced from 22.12% to 2.22%. By providing a robust solution for polarization efficiency optimization in optical systems utilizing freeform LPIOs, this work establishes a solid foundation for advancing the application of freeform LPIOs in optics and photonics.

2. Methods

2.1 Theory of 4×4 method

The 4×4 matrix method, originally introduced by Berreman, is employed to simulate the electromagnetic field distribution as light propagates through an anisotropic medium [8,9]. For liquid crystals characterized by an ordinary refractive index n_o and an extraordinary refractive index n_e, the dielectric tensor, corresponding to a liquid crystal director orientation (n_x, n_y, n_z), is expressed as shown in equation 1:

$$\vec{\varepsilon} = \begin{pmatrix} \varepsilon_\perp + \Delta\varepsilon n_x^2 & \Delta\varepsilon n_x n_y & \Delta\varepsilon n_x n_z \\ \Delta\varepsilon n_x n_y & \varepsilon_\perp + \Delta\varepsilon n_y^2 & \Delta\varepsilon n_y n_z \\ \Delta\varepsilon n_x n_z & \Delta\varepsilon n_y n_z & \varepsilon_\perp + \Delta\varepsilon n_z^2 \end{pmatrix} \quad (1)$$

Here, $\varepsilon_\perp = n_o^2$, $\Delta\varepsilon = n_e{}^2 - n_o^2$. Derived from Maxwell's equations, the relationship governing the electromagnetic field distribution along the z direction is given by:

$$\frac{\partial\vec{\Psi}(z)}{\partial z} = \frac{iw}{c}\vec{D}(z)\vec{\Psi}(z) \quad (2)$$

In above equation, Berreman vector is defined as $\vec{\Psi}(z) = (E_x, \sqrt{\frac{\mu_0}{\varepsilon_0}}H_y, E_y, \sqrt{\frac{\mu_0}{\varepsilon_0}}H_x)^T$, and the equation of $\vec{D}$ is:

$$\vec{D} = \begin{pmatrix} -\frac{\varepsilon_{31}}{\varepsilon_{33}}\frac{ck_x}{\omega} & 1-\frac{1}{\varepsilon_{33}}\frac{c^2k_x^2}{\omega^2} & -\frac{\varepsilon_{32}}{\varepsilon_{33}}\frac{ck_x}{\omega} & 0 \\ \varepsilon_{11}-\frac{\varepsilon_{13}\varepsilon_{31}}{\varepsilon_{33}} & -\frac{\varepsilon_{13}}{\varepsilon_{33}}\frac{ck_x}{\omega} & \varepsilon_{12}-\frac{\varepsilon_{13}\varepsilon_{32}}{\varepsilon_{33}} & 0 \\ 0 & 0 & 0 & -1 \\ -\varepsilon_{21}+\frac{\varepsilon_{23}\varepsilon_{31}}{\varepsilon_{33}} & \frac{\varepsilon_{23}}{\varepsilon_{33}}\frac{ck_x}{\omega} & -\varepsilon_{22}+\frac{\varepsilon_{23}\varepsilon_{32}}{\varepsilon_{33}}+\frac{c^2k_x^2}{\omega^2} & 0 \end{pmatrix} \quad (3)$$

Where, E_x and E_y represent electric field components, while H_x and H_y denote magnetic field components, ε_0 and μ_0 are the vacuum permittivity and permeability, respectively, and ε_{ij} is the dielectric tensor of the medium, as shown in equation (1). Additionally, c is the is the speed of light, ω is the angular frequency of light, and k_x is the wave vector in the x direction.

When $\vec{D}$ does not change from z to $z+\Delta z$, the solution to equation (2) can be expressed as follows:

$$\vec{\Psi}(z+\Delta z) = e\exp(-ik_o\vec{D}(z)\Delta z)\cdot\vec{\Psi}(z) = \vec{P}(z)\cdot\vec{\Psi}(z). \quad (4)$$

For the cholesteric liquid crystals illustrated in figure 1(a), $\vec{D}$ can be considered constant when Δz is much smaller than the pitch of

ISSN 0097-996X/25/5602-1290-$1.00 © 2025

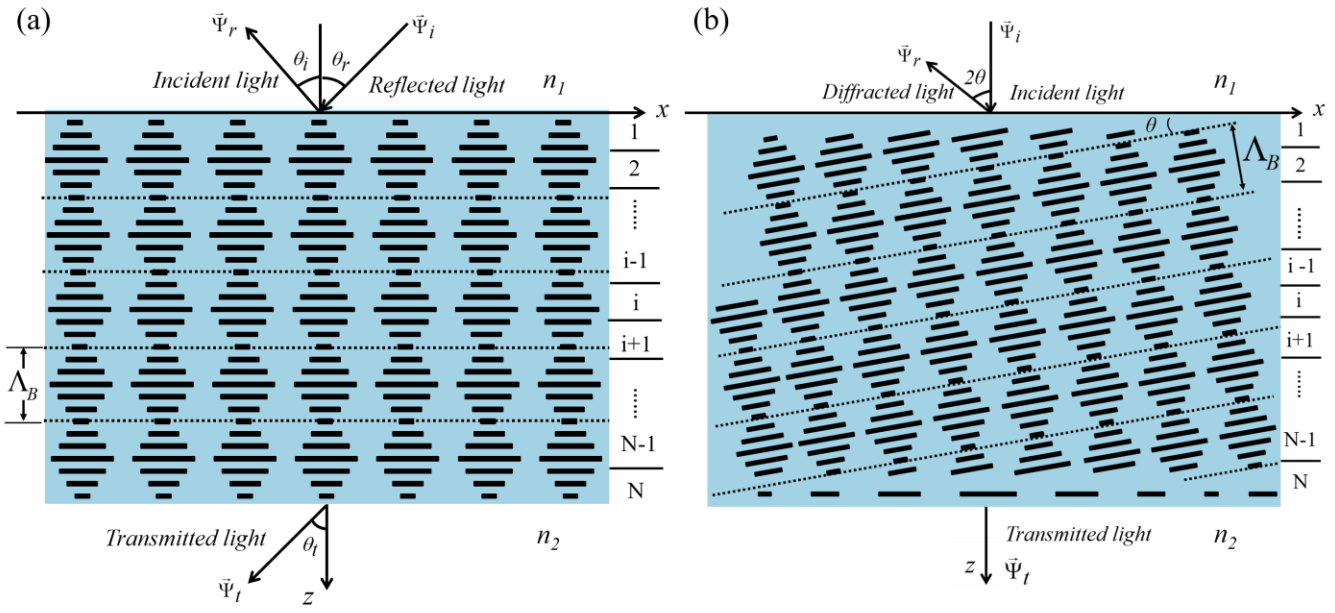

Figure 1. The liquid-crystal structure of (a) cholesteric liquid crystals and (b) reflective liquid-crystal polarization grating.

the cholesteric liquid crystals [10]. Therefore, the Berreman vector of outgoing light can be calculated as:

$$\vec{\Psi}_t = \prod_{i=1}^{N} \vec{P}(i\Delta z)\cdot(\vec{\Psi}_i + \vec{\Psi}_r) = \vec{F}\cdot(\vec{\Psi}_i + \vec{\Psi}_r). \tag{5}$$

Where, N is slab numbers, $\vec{\Psi}_i$ and $\vec{\Psi}_i$ are the Berreman vector of incident light and reflected light, with

$$\begin{cases} \vec{\Psi}_i = (E_{ip}\cos\theta_i, E_{ip}n, E_{is}, -E_{is}n\cos\theta_i)^T \\ \vec{\Psi}_r = (E_{rp}\cos\theta_r, -E_{rp}n, E_{rs}, E_{rs}n\cos\theta_r)^T \\ \vec{\Psi}_t = (E_{tp}\cos\theta_t, E_{tp}n, E_{ts}, -E_{ts}n\cos\theta_t)^T \end{cases}$$

Equation (5) can be reformulated as $\vec{\Psi}_t - \vec{F}\Psi_r = \vec{F}\Psi_i$, and after further derivation, we obtain the following:

$$\vec{G}\begin{pmatrix} E_{tp} \\ E_{ts} \\ E_{rp} \\ E_{rs} \end{pmatrix} = \vec{H}\begin{pmatrix} E_{ip} \\ E_{is} \end{pmatrix} \tag{6}$$

Where,

$$\vec{G} = \begin{pmatrix} \cos\theta_t & 0 & -F_{11}\cos\theta_r + F_{12}n_1 & F_{14}n_1\cos\theta_r - F_{13} \\ n_2 & 0 & -F_{21}\cos\theta_r + F_{22}n_1 & F_{24}n_1\cos\theta_r - F_{23} \\ 0 & 1 & -F_{31}\cos\theta_r + F_{32}n_1 & F_{34}n_1\cos\theta_r - F_{33} \\ 0 & n_2\cos\theta_t & -F_{41}\cos\theta_r + F_{42}n_1 & F_{44}n_1\cos\theta_r - F_{43} \end{pmatrix},$$

$$\vec{H} = \begin{pmatrix} F_{11}\cos\theta_i + F_{12}n_1 & F_{13} - F_{14}n_1\cos\theta_i \\ F_{21}\cos\theta_i + F_{22}n_1 & F_{23} - F_{24}n_1\cos\theta_i \\ F_{31}\cos\theta_i + F_{32}n_1 & F_{33} - F_{34}n_1\cos\theta_i \\ F_{41}\cos\theta_i + F_{42}n_1 & F_{43} - F_{44}n_1\cos\theta_i \end{pmatrix}.$$

After we get the $[E_{tp}, E_{ts}, E_{rp}, E_{rs}]^T$, the diffracted efficiency for specified ray can be calculated as:

$$\eta = \frac{E_{rp}{}^2 + E_{rs}{}^2}{E_{ip}{}^2 + E_{is}{}^2} \tag{7}$$

The liquid-crystal structure of a reflective liquid-crystal polarization grating is illustrated in figure 1(b). For a reflective liquid-crystal polarization grating with grating angle of θ, the diffraction angle for normal incidence is 2θ. The Bragg period of reflective liquid-crystal polarization grating is expressed as

$$\Lambda_B = \frac{\lambda_{in}}{2n_{eff}\cos\theta} \tag{8}$$

Where, λ_{in} is the incident wavelength and n_{eff} is effective refractive index of liquid-crystal, defined as $n_{eff} = \sqrt{(n_e^2 + 2n_o^2)/3}$.

By rotating the x-z coordinate plane by an angle θ, the normal incidence on the liquid-crystal polarization grating can be considered as an oblique incidence in the cholesteric liquid crystals with the same Bragg period. This transformation allows the use of modified 4×4 matrix method to simulate the polarization of light emitted from reflective LPIOs.

2.2 The verification of 4×4 matrix module

To validate the accuracy of 4×4 matrix module, we compared its simulation results with FEM and experimental data. The wavelength is set as 550nm, with the refractive indices of liquid-crystal are n_e = 1.7, n_o = 1.5. The refractive indices of incident medium and transmissive medium are n_1 = 1.57 and n_2 = 1.57. The thickness of the LPIO is 4um, and the slab numbers is N = 4000. The Bragg diffraction angle for the normal incidence is separately set as 20°and 40°. Figures 2(a) and 2(b) show the relationship between the angle of incidence and the diffraction efficiency for different diffraction angles, as determined by the 4×4 matrix module and FEM. For the bandwidth of LPIO with diffraction angle of 40°， the results of FEM and 4×4 matrix module are 23.81° and 22.4°, shows the accuracy of efficiency simulation.

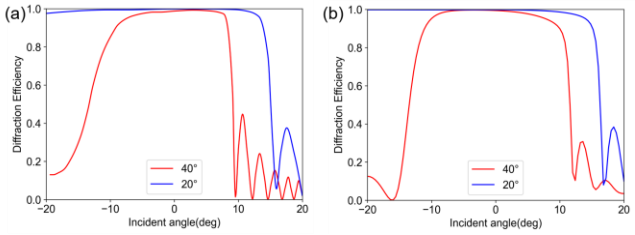

Figure 2. The relationship between the angle of incidence and the diffraction efficiency for different diffraction angles. (a) FEM (b) 4×4 matrix module.

Figure 3 presents the relationship between the angle of incidence and the emitted light polarization using 4×4 matrix module and experimental data for the LPIO with the diffraction angle of 40° in the air. The max S3 deviation of improved 4×4 matrix from experimental data is 3.4% when incident angle is 20°, which is acceptable in the simulation of system efficiency.

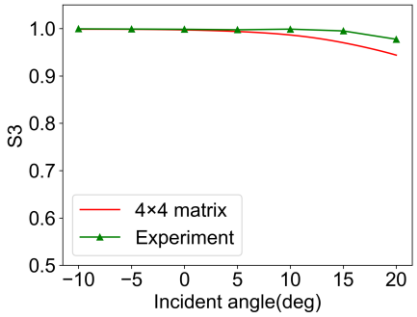

Figure 3. The relationship between the angle of incidence and the emitted light polarization using 4×4 matrix module and experimental data.

2.3 Implementation of polarization efficiency optimization

Since the freeform LPIOs can be regarded as a combination of local reflective LPIOs [4], the polarization ray tracing can be realized in commercial optical software using dynamic link library. Through polarization ray tracing, we can calculate the polarization state of emitted light at different elements in the optical system, therefore the efficiency of ray defined by specific field of view and specific pupil is given by

$$\eta = \frac{E_{out\_p}{}^2 + E_{out\_s}{}^2}{E_{in\_p}{}^2 + E_{in\_s}{}^2} \tag{9}$$

Here, E_{out_p} and E_{out_s} represents the final polarization state of polarization ray tracing, E_{in_p} and E_{in_s} represents the initial polarization state of polarization ray tracing. By sampling the pupil within the field of view, the average efficiency for a specific field can be calculated. Similarly, sampling across the entire field of view allows for the determination of the average efficiency and efficiency uniformity of the system. By optimizing the phase function, Bragg period of the freeform LPIO and other variants in the optical systems, with average efficiency and field uniformity set as constraints, higher efficiency and improved field uniformity can be achieved by modulating the polarization state of light during its propagation through the optical system. Next, we will use an instance of AR display system to verify the impact of polarization efficiency optimization in optical systems utilizing freeform LPIOs.

3. Results

To evaluate the impact of polarization efficiency optimization in an optical system utilizing the freeform LPIOs, we designed an AR display system with and without polarization efficiency optimization. The parameters of the AR system are presented in Table 1.

Table 1. The Parameters of AR display system

Parameters	Value
Field of view	16°×12°
Exit pupil	4mm×3mm
Eye relief	40mm
Image distance	2m
Image source	LCD (11.264mm×8.448mm)
Resolution	1024×768
Wavelength	532nm
MTF	>0.2@45*lp/mm*

As illustrated in figure 4(a), the system consists of two freeform LPIOs and a spherical mirror. The two freeform LPIOs are integrated onto the same substrate to facilitate alignment. The thickness of freeform LPIOs is set to 4um with slab numbers same as above. The refractive indices of liquid-crystal are n_e = 1.655 and n_o = 1.55. The metallic mirror is modeled as silver (Ag, n = 0.051781 + 3.4215j), and the polarization state of the emitted light is calculated using Fresnel's equations.

For the display system without polarization efficiency optimization, the modulation transfer function (MTF) curve exceeds 0.2 at 45 *lp/mm*, as shown in figure 4(b). Despite the highly oblique characteristics of display system, distortion is reduced to below 5%, as depicted in figure 4(c). The Λ_B is set as 173.68nm to ensure the primary ray of central field satisfies Bragg condition. The system achieves an average efficiency of 59.16% with a uniformity of 22.12%, as illustrated in figure 4(d).

For the display system with polarization efficiency optimization, through the optimization of the phase function and Bragg period of freeform LPIO and other variants in the display system, a similar layout, MTF curve, and distortion are maintained, as shown in figures 4(e), 4(f), and 4(g). However, the system's efficiency significantly increases from 59.16% to 88.29%, and the field uniformity improves dramatically from 22.12% to 2.22%, as demonstrated in figure 4(h).

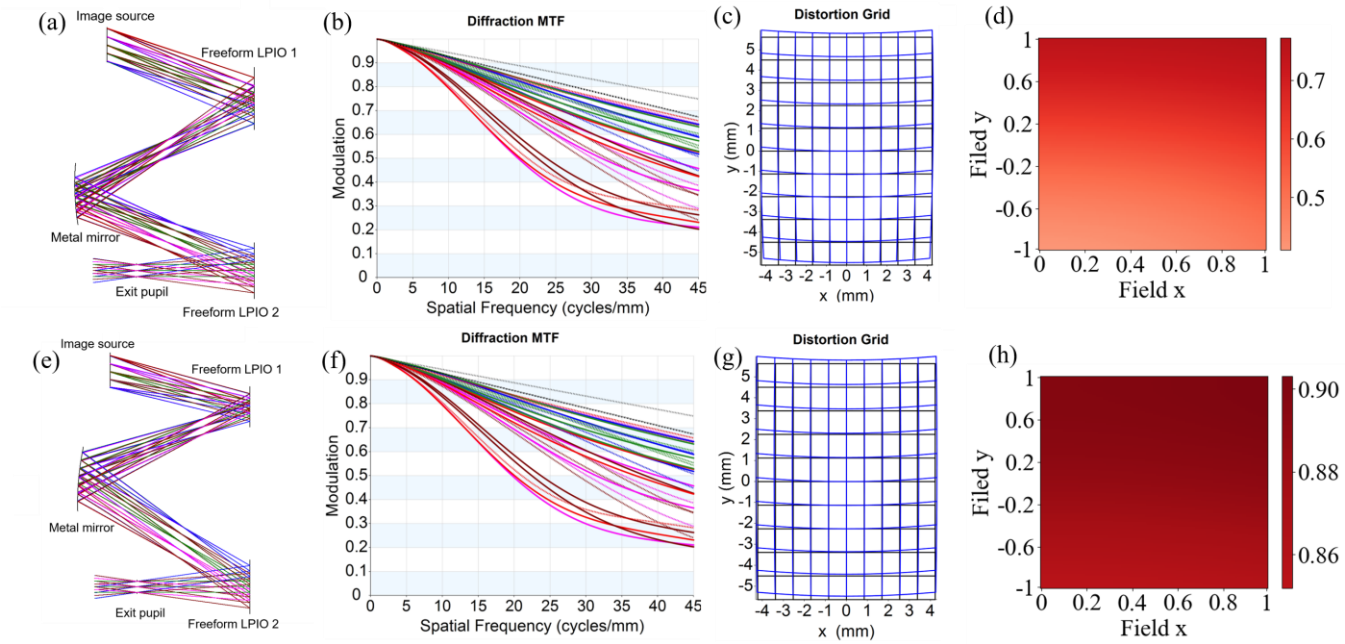

Figure 4. The simulation results of optimized AR display system. For system without the polarization efficiency optimization (a) The configuration layout, (b) The MTF curve, (c) Distortion gird and (f) The distribution of diffraction efficiency within the whole field of view. And (e),(f),(g),(h) is the corresponding simulation results for system incorporating polarization efficiency optimization.

4. Conclusion

In summary, we developed an approach for polarization efficiency optimization of freeform LPIOs. The accuracy of the emitted light polarization was validated through comparation with simulation results of FEM and experimental data. Additionally, a self-built 4×4 matrix module was implemented in commercial optical software via a dynamic link library to realize the polarization ray tracing of freeform LPIOs.

Compared with systems lacking polarization efficiency optimization, the system incorporating polarization efficiency optimization demonstrated a 28.68% improvement in average efficiency alongside enhanced field uniformity, highlighting the necessity of polarization efficiency optimization for freeform LPIOs. This work shows significant potential in LPIO-based applications requiring polarization management, such as waveguide display systems and head-up displays, offering an effective solution to fully exploit the bandwidth of freeform LPIOs.

5. Acknowledgements

This work was supported by the National Key R&D Program of China (No. 2021YFB2802200) and the National Natural Science Foundation of China (No. 12074338).

6. References

[1] Kobashi J, Yoshida H, Ozaki M. Planar optics with patterned chiral liquid crystals[J]. Nat. Photonics, 2016, 10(6):389–92.

[2] Weng Y, Xu D, Zhang Y, Li X, Wu S-T. Polarization volume grating with high efficiency and large diffraction angle[J]. Opt. Express, 2016, 24(16):17746–17759.

[3] Weng J, Li H, Wu R, Liu X. Single-image-source binocular waveguide display based on polarization volume gratings and lenses[J]. Opt. Lett, 2023, 48(8):2050–2053.

[4] Pei C, Weng J, Shu T, Fang L, Hu G, Liu Y et al. Freeform Liquid–Crystal Polarization Imaging Optics: A Practical Approach from Design to Fabrication[J]. Laser Photon. Rev., 2024, 18(9).

[5] Yariv A, Yeh P. Optical Waves in Crystals: Propagation and Control of Laser Radiation, Wiley, New York 1984.

[6] Weng Y, Xu D, Zhang Y, Xiao L, Wu S-T. Polarization volume grating with high efficiency and large diffraction angle[J]. Opt. Express, 2016, 24(16):17746–17759.

[7] Liu S, Yu H, Jiang M, Feng J, Wei Q-H, Numerical study of transmissive liquid crystal Pancharatnam–Berry gratings with small periods, J. Opt. Soc. Am. B., 2023, 40(2), 431-435.

[8] Berreman D W. Optics in Stratified and Anisotropic Media: 4 X 4-Matrix Formulation[J]. J. Opt. Soc. Am, 1971, 62(4): 502-510.

[9] Berreman D W. Optics in smoothly varying anisotropic planar structures: Application to liquid-crystal twist cells[J]. J. Opt. Soc. Am., 1973, 63(11): 1374-1380.

[10] Ozaki R, Nakahiro K. Electric field analysis in chiral liquid crystals by Berreman's 4 × 4 matrix method[J]. Jpn. J. Appl. Phys., 2022, 61(6):61006.